

The α particle based on modern nuclear forces

A. Nogga¹, H. Kamada², W. Glöckle³, B.R. Barrett¹

¹*Department of Physics, University of Arizona, Tucson, Arizona 85721, USA*

²*Department of Physics, Faculty of Engineering,*

Kyushu Institute of Technology, Kitakyushu 804-8550, Japan

³*Institut für theoretische Physik II, Ruhr-Universität Bochum, D-44780 Bochum, Germany*

(Dated: October 30, 2018)

The Faddeev-Yakubovsky equations for the α particle are solved. Accurate results are obtained for several modern NN interaction models, which include charge-symmetry breaking effects in the NN force, nucleon mass dependences as well as the Coulomb interaction. These models are augmented by three-nucleon forces of different types and adjusted to the 3N binding energy. Our results are close to the experimental binding energy with a slight overbinding. Thus there is only little room left for the contribution of possible 4N interactions to the α particle binding energy. We also discuss model dependences of the binding energies and the wave functions.

PACS numbers: PACS numbers: 21.10.-h, 21.45.+v, 27.10.+h, 21.30.-x

I. INTRODUCTION

In spite of the tremendously increased computational power of today's super computers, numerical investigations of nuclear bound states are still a challenging problem, even for systems of few nucleons. Investigations promise insights into the rich structure of nuclear interactions. To this aim one requires reliable solutions of the dynamical equations. In this article we would like to present results for the α particle, which are based on realistic microscopic nuclear forces including three-body interactions.

In recent years forces could be adjusted accurately to the huge amount of available NN low energy scattering data [1, 2, 3]. The overall agreement of the predictions of these model forces with the data is essentially perfect. As a result it has been shown that most of the observables in the low energy regime of the 3N continuum could be predicted model independently [4, 5], though the interactions themselves are quite different. On the other side, it is known since quite a long time that the 3N binding energies (BE) are quite model dependent and, moreover, are generally smaller than the experimental value [6, 7, 8, 9]. It is assumed that most of this underbinding is due to three-nucleon forces (3NF) and modifications of the NN interaction in the presence of a third nucleon. The latter one is of course also part of a three-nucleon force mechanism.

The nature of these 3NF's is still not completely understood. It is clear that such forces should already arise because of the composite structure of the nucleons, what is partially taken into account by allowing for intermediate Δ -excitation. Other mechanisms of various meson-exchange types will also contribute (for a review see [10]). In recent years there has been new progress in understanding the form of nuclear forces, because of the application of chiral perturbation theory (χ PT) [11, 12, 13, 14, 15, 16, 17]. From this developments one can expect a more systematic understanding of the form of NN and 3N forces in the near future. However, χ PT implies *a priori* unknown constants, the low-energy constants, which have to be determined from experimental data. The bound states of few-nucleons seem to be an ideal laboratory to determine 3NF parameters, as the BE's are sensitive to the 3N interaction and they are expected to be governed by the low-energy regime of nuclear physics [18]. Therefore, the understanding of nuclear bound states is an important contribution to the understanding of the 3NF.

At present these chiral interactions are not as accurate as the traditional, phenomenological NN forces [1, 2, 3]. At the order of the chiral expansion parameter considered up to now [19], they do not yet describe the NN phase shifts with the same accuracy. Allowing, however, for additional fine tuning a high accuracy description can be achieved [20]. The aim of this article is to pin down model dependences of predictions for the α particle BE and wave function (WF) properties. To insure that differences in the predictions are not due to an inaccurate description of the NN system, but are due to the more fundamental differences of the interaction models, we restrict ourselves to the traditional models in this paper. The techniques developed, however, will help to apply also the upcoming chiral interactions. First investigations, using chiral interactions, have already been undertaken [19, 21].

Our approach leads immediately to a basic problem. It has been shown that the 3N interaction cannot be determined uniquely and, moreover, that each NN interaction has to be accompanied by a different 3NF [22]. For the traditional NN interactions, there are no 3NF's available, which have been derived consistently to them. Therefore, we have to rely on 3NF's, which just take parts of the mechanisms into account, which are expected to contribute to the 3NF. These models are, for example, the Tucson-Melbourne (TM) [23] and the Urbana IX (Urb-IX) [24] 3NF's. For the different NN interactions these models have been adjusted separately to the experimental ^3H BE, as described in Section III A. This scheme is justified for two reasons:

- It has been shown that many 3N scattering observables in the low energy regime (below ≈ 10 MeV nucleon lab energy) scale with the ${}^3\text{H}$ BE. This means that predictions for different model Hamiltonians are equal, when the models predict the same ${}^3\text{H}$ BE [25, 26, 27]. An adjustment of the 3NF's exclude model dependences related to this phenomenon. We will see that these effects are also visible for the α particle.
- In the high energy regime (above ≈ 100 MeV nucleon lab energy) the predictions for 3N scattering observables are sensitive to the 3NF showing that the available 3NF models are quite different [5]. This insures that the models applied in this paper cover a wide range of possible 3NF's. Therefore, our results show the model dependences of our current understanding of the α particle, which are related to the structure of the 3NF.

Bound states of light nuclei have been investigated by several groups using different techniques [28, 29, 30, 31, 32, 33, 34, 35, 36, 37, 38]. But much of the work is still restricted to somewhat simplified interactions. Perhaps the most advanced calculations covering several nuclei have been performed by the Argonne-Los Alamos collaboration [28, 29]. Using the Greens functions Monte Carlo (GFMC) technique, they were able to predict BE's for the light nuclei up to $A = 8$. However, their work is restricted to the AV18 NN interaction model and the class of Urb-IX 3NF's (new terms not considered here have been added in [29]). This leads to the question, whether the other available interactions give similar or different results for these nuclei. In this respect the “no-core” shell model approach (NCSM) [30] might be more flexible. But the work on 3NF's has not been finished yet. Therefore, we think that a study of the 4N system can provide important new information on the nuclear interactions, if one can investigate a wide range of NN and 3N models in this system.

In this paper we use the Faddeev-Yakubovsky scheme to solve the non-relativistic Schrödinger equation (SE) for four nucleons. This has been started already in Refs. [36, 39, 40, 41, 42, 43]. With this method we are able to get reliable results for the BE and the WF of the α particle for several NN and 3N interactions. The calculations are restricted to $A = 3$ and $A = 4$, but we were able to pin down the dependence on today's interaction models. The highly accurate WF, which result from the calculations, are necessary for the analysis of several on-going or planned experiments on the α particle, which might reveal the short-range correlations in nuclei [44] or give insights into the charge independence breaking of the nuclear interaction [45]. Exact WF's are also necessary to understand the results of parity violating e^- scattering experiments [46]. Therefore, we will also give first results of calculations including the isospin $T = 1$ and $T = 2$ component of the α particle ground state WF.

Another important issue is a first estimate of the size of a possible 4N interaction. We expect that it should show up especially prominent in the α particle, because of its high density. Our calculations give some hints, as to whether there is room for an important contribution of the 4N interaction in nuclei given today's NN and 3N interaction models.

In Section II we briefly review the 4N Faddeev-Yakubovsky formalism. The calculations are based on adjusted 3NF's. The adjustment procedure is described in Section III A. Our results for the BE's of the α particle based on various nuclear force combinations are given in Section III B and the properties of the obtained WF's are presented in Section III C. Finally we summarize in Section IV.

II. THE 4N YAKUBOVSKY FORMALISM

The technical challenge in all investigations of nuclear bound states is the accurate inclusion of all short-range correlations in the nuclear WF. Due to these short-range correlations, the partial wave decomposition of nuclear WF's is very slowly converging. This hold especially for the very tightly bound α particle WF. Therefore, a rewriting of the Schrödinger equation for the 4N system

$$H \Psi = \left(T + \sum_{i < j} V_{ij} + \sum_{i < j < k} V_{ijk} \right) \Psi = E \Psi \quad (1)$$

according to the formalism of Yakubovsky [47] is useful. We take NN pair potentials V_{ij} and 3N potentials V_{ijk} into account. T denotes the kinetic energy operator, H the full 4N Hamiltonian and Ψ the 4N WF. We will use Jacobi coordinates (see Fig. 1) to represent our WF and dynamical equations. These separate the center of mass motion and, at the same time, guarantee a kinetic energy operator independent from angular variables. But these coordinates do not include *all* kinds of pair coordinates at the same time and it is hard to describe the short range correlations of pairs in other coordinates than their own relative coordinate. Other coordinates unavoidably lead to strong angular dependences or, in other words, to a very slowly converging series of partial waves. On the other hand, the Jacobi coordinates include the relative coordinates of *some* pairs. Correlations of those pairs are easily described. The WF contains the correlations of all pairs and is hard to expand in Jacobi coordinates. This makes the decomposition of

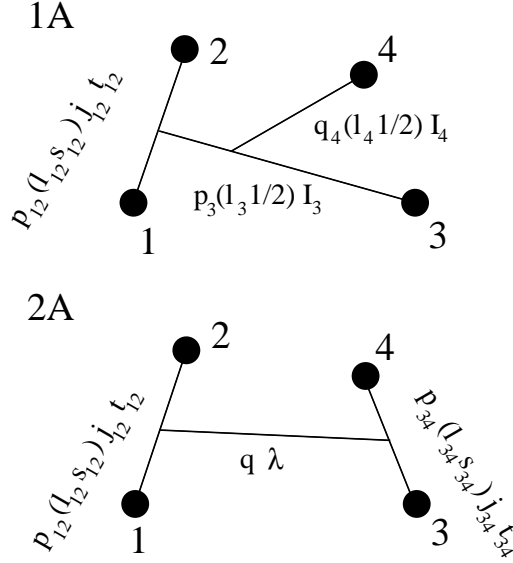


FIG. 1: Definition of the 1A and 2A type of Jacobi coordinates.

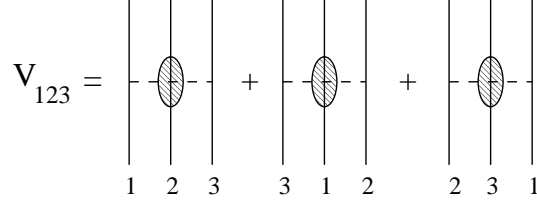


FIG. 2: The three parts of a meson exchange 3NF, which differ only by an exchange of the particles.

the WF in Yakubovsky components (YC) highly advisable. The YC's single out clusters of the four particles. The way they are defined guarantees that they are driven by correlations within these clusters only. Therefore, they are efficiently expanded in Jacobi coordinates, which single out the same clusters.

In the isospin formalism nucleons are identical particles. This implies several symmetry properties, which connect the different YC's and reduce the number of independent coupled equations and YC's to two. The following set of Yakubovsky equations (YE's) are obtained for the two YC's ψ_{1A} and ψ_{2A} [36, 39, 48]

$$\psi_{1A} \equiv \psi_{(12)3,4} = G_0 t_{12} P [(1 - P_{34}) \psi_{1A} + \psi_{2A}] + (1 + G_0 t_{12}) G_0 V_{123}^{(3)} \Psi \quad (2)$$

$$\psi_{2A} \equiv \psi_{(12)34} = G_0 t_{12} \tilde{P} [(1 - P_{34}) \psi_{1A} + \psi_{2A}] \quad (3)$$

The other YC's are replaced by transposition operators P_{ij} and combinations $P = P_{13}P_{23} + P_{12}P_{23}$ and $\tilde{P} = P_{13}P_{24}$, acting on the two remaining YC's. The kinetic energy enters through the free propagator $G_0 = \frac{1}{E-T}$ and the pair interaction by means of the pair t -matrix t_{12} . The 3NF's show up in the interaction term $V_{123}^{(3)}$. This defines a part of the 3NF in the cluster (123), which is symmetric in the pair (12) and which can be related by an interchange of the three particles to two other parts $V_{123}^{(1)}$ and $V_{123}^{(2)}$ that sum up to the total 3NF of particles 1,2 and 3: $V_{123} = V_{123}^{(1)} + V_{123}^{(2)} + V_{123}^{(3)}$. For 3NF's based on a meson-exchange picture, $V_{123}^{(3)}$ describes the interaction induced by a meson interchanged between particles 1 and 2 and, on the way, re-scattered by the third particle, as indicated in Fig. 2.

Applying a combination of transpositions to the set of YC's, one obtains the WF as

$$\Psi = [1 - (1 + P)P_{34}](1 + P)\psi_{1A} + (1 + P)(1 + \tilde{P})\psi_{2A} \quad (4)$$

The YC's ψ_{1A} and ψ_{2A} are anti-symmetric in the pairs (12) or (12) and (34), respectively [48]. This guarantees the total anti-symmetry of the WF Ψ .

The YC's are expanded in their "natural" Jacobi coordinates. This means that ψ_{1A} is represented in the coordinates shown in the top of Fig. 1, because both single out the pair (12) and the cluster (123). ψ_{2A} singles out both pairs, (12)

and (34), and is simplest, when expanded in the coordinates, shown at the bottom of Fig. 1. Each of the coordinates involves three relative momenta p_{12} , p_3 and q_4 or p_{12} , p_{34} and q , respectively. The angular dependence is expanded in partial waves, leading to three orbital angular momentum quantum numbers for each kind of coordinate: l_{12} , l_3 and l_4 or l_{12} , l_{34} and λ . We use jj coupling. Therefore, we couple, as indicated in the figure, the orbital angular momenta and corresponding spin quantum numbers to the intermediate quantum numbers j_{12} , I_3 and I_4 or j_{12} and j_{34} , and these are coupled to the total angular momentum J and its third component M , using two additional intermediate angular momenta j_3 and I : $((j_{12}I_3)j_3I_4)JM$ or $((j_{12}\lambda)Ij_{34})JM$. For the isospin quantum numbers (see Fig. 1) similar coupling schemes to total isospin TM_T involve only one intermediate quantum number τ : $((t_{12} \frac{1}{2})\tau \frac{1}{2})TM_T$ or $(t_{12}t_{34})TM_T$.

As we already pointed out, the partial wave decomposition requires a huge number of partial waves, whenever one needs to represent correlations of pairs and clusters in coordinates, which don't single them out. Unfortunately, this is still necessary in the intermediate states in Eqs. (2) and (3) (for $P \psi_{1A}$, etc.). Therefore, we still need a tremendous number of partial waves to find converged results. However, we are going to show numerically in Section III B that we can speed up the convergence greatly by using the Yakubovsky decomposition. For our calculations, we decided to truncate the orbital angular momenta, requiring that $j_{ij} \leq 6$ and $l_i, \lambda \leq 8$. Additionally, we constrain the expansion for both kinds of coordinates by another parameter l_{sum}^{max} , requiring that $l_{12} + l_3 + l_4 \leq l_{sum}^{max}$ and $l_{12} + l_{34} + \lambda \leq l_{sum}^{max}$.

We use $l_{sum}^{max} = 14$. Our most sophisticated calculations, including the $T = 1$ and $T = 2$ isospin channels, need a total number of 4200 partial waves for the first kind of coordinates and 2000 for the second kind. We require 36-40 mesh points to discretize the magnitudes of each of the momenta p_{12} , p_3 and q_4 or p_{12} , p_{34} and q . This insures that we obtain results for the binding energy of the α particle, which are converged within 50 keV.

Using this partial wave truncation, we find that the discretized integral kernel for the set of Eqs. (2) and (3) is of the dimension $3 \cdot 10^8 \times 3 \cdot 10^8$. Clearly this can no longer be treated by standard techniques of numerical linear algebra, like the QR-algorithm, and one is forced to use an iterative scheme. A Lanczos type method [8, 49] has turned out to be very powerful in the past and also here. Succinctly, for an arbitrary N -component starting vector for the unknown amplitude, one applies the kernel leading to a new vector. This is repeated several times by applying the kernel always to the new vectors. That set of vectors is then orthonormalized and the unknown amplitude expanded into those elements. Inserting this expansion again into the eigenvalue equation Eqs. (2) and (3), one ends up with a small set of linear algebraic eigenvalue equations of dimension n , where n counts the number of applications of the kernel. n is typically 10-20. The energy eigenvalue E , which is buried as a parameter in the kernel is determined in such a manner that the eigenvalue of the kernel is 1.

Another challenge is the application of the three-nucleon force. In momentum space and partial-wave decomposed, this is a huge matrix of typical dimension $5 \times 10^4 \times 5 \times 10^4$ for each total 3N angular momentum and parity. In case of the α particle, the 3N subsystem total angular momenta have to be taken into account up to $\frac{17}{2}$. Instead of preparing these matrices, we handle the 3N forces differently. They can be naturally broken up into a sequence of pseudo two-body forces with a change of Jacobi momenta in between (transpositions). This has been described, for the first time in [50]. The generalization to the 4N system is described in Appendix B. This technique is much more efficient and even allows one to evaluate the 3NF's in each new iteration of the kernel – no storage of huge intermediate matrices related to 3NF's is required.

A typical run on a massively parallel T3E with 128 processors takes 2 hrs to get one eigenvalue and the corresponding eigenvector. For our method of parallelization we refer to [51].

III. RESULTS

A. Adjustment of 3NF's

In this paper we restrict ourselves to the modern realistic NN interactions, which are all fitted to the NN data with the same high accuracy and also provide a nn force, which predicts a reasonable nn scattering length. These interactions are the AV18 [2] and the CD-Bonn [1]. Additionally we show results for the Nijm I, Nijm II and Nijm 93 interactions [3], which are not adjusted to the nn scattering length and in case of Nijm 93 give a slightly less accurate fit to the NN data. The results for the ^3He and ^3H BE's are shown in Table I. They are based on calculations, which take two-body angular momenta up to $j_{12} = 6$ into account and are converged up to 2 keV. The full charge dependence of the interaction as well as the n-p mass difference are considered. Also the Coulomb force is included exactly as described in [37, 51].

As well known [7, 8, 52, 53, 54] all NN model interactions lead to an underpredicted 3N BE. The underprediction is strongly model dependent and ranges from 0.8 MeV to 0.5 MeV for the most modern interactions (see Table I) though their description of the NN data is comparable. For benchmark purposes, we also show results for the expectation value of the kinetic energy. These tend to be smaller for the non-local interaction Nijm I and CD-Bonn. This behavior can be

interaction	${}^3\text{H}$		${}^3\text{He}$		ΔE_B
	E_B	T	E_B	T	
CD-Bonn	-8.013	37.43	-7.288	36.62	0.725
AV18	-7.628	46.76	-6.917	45.69	0.711
Nijm I	-7.741	40.74	-7.083	40.01	0.658
Nijm II	-7.659	47.55	-7.008	46.67	0.651
Nijm 93	-7.668	45.65	-7.014	44.79	0.654
Exp.	-8.482	—	-7.718	—	0.764

TABLE I: 3N binding energies E_B for different NN interactions compared to the experimental values. Results are shown for ${}^3\text{H}$, ${}^3\text{He}$ and their binding energy difference ΔE_B . Additionally, we show the kinetic energies T . All results are given in MeV

traced back to the softer repulsive core of non-local NN forces. We also show the binding energy difference of the two mirror nuclei ΔE_B . One sees that all models underpredict the experimental value. The deviation is somehow larger for the Nijmegen interactions, which do not describe the nn scattering length correctly. The additional differences for the Nijmegen interactions are, therefore, likely a result of an inadequate description of the NN scattering data. We will address the issue of the ${}^3\text{H}$ - ${}^3\text{He}$ binding energy difference in Ref. [55]; therefore, we do not want to go in details here.

Two possible dynamical ingredients are still missing in our calculations: relativistic effects and 3NF's. We will not address the interesting question of including relativity in few-nucleon dynamics here. Attempts to understand this issue can be found in Refs. [56, 57, 58, 59, 60, 61]. The results of those calculations are varying. Whereas approaches based on field equations, like Bethe-Salpeter or Gross equations generally predict an increased binding energy compared to the non-relativistic solution, the calculations based on a relativistic Schrödinger equation predict a decreased binding energy. In the latter case the relativistic effects are driven by boost properties, whereas in field theoretical approaches additional dynamical effects also occur. The magnitude of the predicted effects is of the order of 200 keV. The problem is not yet solved. It has also been observed that relativistic effects and 3NF effects are related and cannot be separated in field equation approaches [59]. In this paper we neglect all relativistic effects, hoping that part of them are included in effective 3NF terms.

The knowledge regarding 3NF's is similarly scarce, as for the relativistic effects. It has been shown in Ref. [22] that 3NF's are not defined independently from the accompanying NN interactions. Two 3N Hamiltonians based on two different, but phase equivalent NN interactions, can be augmented by a properly chosen 3N interaction to be equivalent in the 3N system. In [37] we formulated the more inclusive statement that one could, in principle, always find NN interactions, which replace a 3N interaction completely in a 3N Hamiltonian. Ref. [22] does not conclude that this is *always* possible. It is clear anyhow that the transformation are complicated and therefore it is not practicable to use them to get rid of the 3NF's. As soon as one includes relativistic features the Poincaré algebra inevitably enforces 3NF's [62], which cannot be transformed away.

In view of this connection of 3NF models and NN force models, a phenomenological approach to the 3NF is justified: given a 3NF model, one adjusts its parameters in conjunction with one NN interaction model to 3N or other nuclear data leading to different parameter sets of the 3NF for each NN interaction.

For the Urb-IX 3NF the parameters have been fixed in conjunction with the AV18 interaction using the ${}^3\text{H}$ BE and the nuclear matter density predicted by this combination [24]. The TM force originally has not been adjusted in this way. Its parameters have been deduced from model assumptions and using πN scattering data [23, 63, 64]. It is clear that a complete 3NF based on meson-exchange should include not only π - π , but also ρ - π , ρ - ρ and so on exchanges. Attempts to include these processes have been done, but conclusive results, fixing the parameter sets, could not be obtained [65]. Therefore, we assume in our study that we can effectively include the effects of heavier mesons in the π - π exchange TM model by a variation of the πNN form factor parameter Λ . It has been observed [8, 66] that the ${}^3\text{H}$ BE is sensitive to this cut-off. The original value $\Lambda = 5.8m_\pi$ has been fixed by matching the Goldberger Treiman discrepancy [64]. However, as has been argued in [67], the form factors are ill-defined, because they strongly influence the long-range part of the 3NF. Therefore an adjustment is justified. We emphasize that the aim of this paper is the investigation of model dependences due to the different 3NF's. To this aim we only require 3NF models, which are different and which have a sufficiently rich spin-isospin dependence. An adjustment of the 3NF does not spoil these requirements.

We combined in Refs. [9, 37] the available NN interactions with the TM 3NF and tuned Λ to reproduce the ${}^3\text{H}$ or ${}^3\text{He}$ BE's. The resulting Λ values are shown in Table II. The table also includes results for a modified TM interaction. It has been argued in [68] that the long-range/short-range part of the c -term is not consistent with chiral symmetry. Dropping it leads to a changed set of parameters, which we refer to as TM'. The parameters of TM and TM' are

interaction	Λ	$E(^3\text{H})$	$E(^3\text{He})$	ΔE_B
CD-Bonn+TM	4.784	-8.478	-7.735	0.743
AV18+TM	5.156	-8.478	-7.733	0.744
AV18+TM'	4.756	-8.448	-7.706	0.742
AV18+Urb-IX	—	-8.484	-7.739	0.745
AV18+Urb-IX (Pisa) [69]	—	-8.485	-7.742	0.743
AV18+Urb-IX (Argonne) [28]	—	-8.47(1)	—	—
Exp.	—	-8.482	-7.718	0.764

TABLE II: 3N binding energy results for different combinations of NN and 3N interactions, together with the adjusted form factor parameters Λ in units of m_π . The binding energies for ^3H $E(^3\text{H})$ and ^3He $E(^3\text{He})$ are shown. For completeness the splitting ΔE_B is also displayed. All energies are given in MeV.

summarized in Table XI of Appendix B.

The fits have been done using less accurate BE calculations not including the isospin $T = \frac{3}{2}$ component and not including the effect of the n-p mass difference. Therefore, the new results for the BE's, shown in the table, do not exactly match the experimental values. The deviations are non-significant for the following study, so we refrain from refitting the Λ 's. We adjusted TM to the ^3H BE and TM' to the ^3He BE. The table also shows our results using the Urb-IX interaction, as defined in [24].

Table II confirms at the same time a well-known scaling behavior of the Coulomb interaction with the BE of ^3He [70]. The adjusted 3N Hamiltonians predict very similar 3N binding energies and ΔE_B 's. This removes the model dependence of ΔE_B found in Table I. We observe that the model independent prediction for these energy difference deviates from the experimental value by about 20 keV. Again, we refer to Ref. [55] for a more detailed discussion of this issue. In the same reference, a detailed comparison with hyper-spherical variational calculations is given. In Table I, for comparison, we only show the BE's obtained by the Pisa and Argonne group. We note that the calculation by the Pisa group is in full agreement with our results. The small deviation from the Argonne result is not significant in view of the comparably large statistical error bar of the GFMC calculation.

We are now ready to apply the 3N model Hamiltonians, given by the Λ values in Table II, to the 4N system. By using the models from Table II, we insure that dependences due to scaling effects, as visible for example in ΔE_B , are excluded. Given the very different functional forms of the Urb-IX, TM and TM' interactions, we can expect to see any remaining model dependences in our calculations.

B. α particle binding energies

Based on these model Hamiltonians, we solved the YE's (2) and (3) with no uncontrolled approximation. The following results are based on a partial wave decomposition truncated using $l_{sum}^{max} = 14$. It has been verified that this is sufficient to obtain converged BE's with an accuracy of 50 keV. The binding energies given were found varying the energy parameter in Eqs. (2) and (3) until the eigenvalue 1 appears in the spectrum of the set of YE's.

Independently, one can check the results with a calculation of the expectation value of the Hamiltonian. We emphasize that this is an important feature of our method, which minimizes the possibility of errors in the codes or unexpected numerical difficulties.

For these checks one faces the problem to represent the WF with high accuracy. We already pointed out that the WF of the α particle is extremely slowly converging, because there is no set of Jacobi momenta suitable to describe the short range correlation in *all* NN pairs. In Table III we exemplify the convergence behavior of the WF for the AV18 interaction. The normalization and the expectation values of the kinetic energy, potential energy and Hamiltonian are shown. The WF's have been derived from the same set of YC's, using Eq. (4). The calculation of the WF is based on a partial wave decomposition truncated with $l_{sum}^{max} = 14$. In this way we obtained the WF in the two different representations, depicted in Fig. 1. For the expectation values shown in the table, we truncated the WF in a second step to the partial waves given by the l_{sum}^{max} parameter in the first column. It turned out that the evaluation of the kinetic energy is difficult, because T amplifies the slowly converging high momentum components of the WF. The kinetic-energy expectation values, shown in the fourth and fifth columns of the table, do not converge within the chosen partial-wave truncation. However, one can rewrite the kinetic energy using Eq. (4) and the fact that the transposition operators commute with the kinetic energy and simply result in a sign change, if applied to a

J_{sum}^{max}	$\langle \Psi \Psi \rangle^{1A}$	$\langle \Psi \Psi \rangle^{2A}$	$\langle \Psi T \Psi \rangle^{1A}$	$\langle \Psi T \Psi \rangle^{2A}$	$T(mix)$	$\langle \Psi V \Psi \rangle^{1A}$	$\langle \Psi V \Psi \rangle^{2A}$	$\langle H \rangle^{1A}$	$\langle H \rangle^{2A}$
2	0.9117	0.9084	61.27	62.14	91.80	-110.20	-110.44	-18.40	-18.65
4	0.9662	0.9582	79.10	76.11	96.85	-117.55	-118.12	-20.70	-21.27
6	0.9820	0.9766	86.36	83.49	97.56	-120.66	-120.71	-23.09	-23.15
8	0.9927	0.9890	92.41	90.09	97.75	-121.43	-121.39	-23.67	-23.63
10	0.9961	0.9939	94.59	92.93	97.79	-121.84	-121.84	-24.05	-24.05
12	0.9982	0.9969	96.10	95.04	97.80	-121.97	-121.96	-24.16	-24.16
14	0.9990	0.9986	96.51	95.70	97.80	-122.03	-122.01	-24.23	-24.21

TABLE III: Convergence of the α particle WF for different truncations of the basis states. The superscripts 1A and 2A indicate the type of Jacobi coordinates employed. The results are based on a calculation using the AV18 NN interaction and no 3NF. See text for details.

interaction	E_α	H	T	V_{NN}
Nijm 93	-24.53	-24.55	95.34	-119.89
Nijm I	-24.98	-24.99	84.19	-109.19
Nijm II	-24.56	-24.55	100.31	-124.86
AV18	-24.25	-24.23	97.80	-122.03
CD-Bonn	-26.26	-26.23	77.15	-103.38
CD-Bonn [30]	-26.4(2)	—	—	—
Exp.	-28.30	—	—	—

TABLE IV: α particle binding energy predictions E_α of several NN potential models compared to the experimental value and the “no-core shell model” result [30]. The expectation values of the kinetic energy T , the NN interaction V_{NN} and the Hamiltonian operator H are also shown. All energies are given in MeV.

fully anti-symmetrized WF:

$$\langle \Psi | T | \Psi \rangle = 12 \langle \Psi | T | \psi_{1A} \rangle + 6 \langle \Psi | T | \psi_{2A} \rangle \quad (5)$$

The right-hand side involves mixed matrix elements with the YC’s. The first term has to be evaluated in the 1A representation, because ψ_{1A} is given in these coordinates, and the second term in the 2A ones because of the coordinates of ψ_{2A} . The results for T based on this equation are shown in the column labeled $T(mix)$ and show a promising convergence behavior. We observe a much faster convergence for the YC’s, which was expected and which justifies the YE’s approach to the 4N Schrödinger equation. Based on this experience, we normalize our WF and the YC’s using a similar formula for the norm. Consequently, the deviation of directly calculated norms of the WF, shown in columns 2 and 3, from one is a measure of the numerical error of our anti-symmetization of the full WF.

Unfortunately, a similar approach is not possible for the expectation values of the potential. However, the interaction does not overemphasize the high-momentum tail and its expectation value is much faster converging. We find a reasonable agreement of 0.02 % of the 1A and 2A results and convergence of both values to uncertainty of 60 keV. For completeness we show the expectation value of the Hamiltonian based on $T(mix)$ and the 1A or 2A expectation value of V . These values agree within 0.1 %. The expectation values differ from the binding energy result of -24.25 MeV by only 20 to 40 keV. This is well within the error of 60 keV, which has to be expected from the convergence behavior of V and verifies the accuracy of our results. In the following, we will only present the binding energies, the $T(mix)$ values and the expectation values of H and V based on the 1A representation. We consider it more accurate than the 2A representation, because the norm is closer to one.

In Table IV our α particle binding energies are summarized for Hamiltonians based on NN forces only. The results are identical to the ones published in Ref. [37] except for AV18, where we present a new calculation, based on a more accurate grid and taking $T = 1$ and $T = 2$ components into account. Due to the more accurate momentum grid, our binding energy changed by 30 keV, well within our estimated numerical error of 50 keV. Therefore, we did not redo the calculation for the other interactions. The table also shows a result obtained using the NCSM approach [30]. Our result agrees with their number within the numerical errors estimated.

As in the case of the 3N BE’s, the 4N BE’s are also underpredicted by all modern NN force models. The underbinding ranges from 2 to 4 MeV, showing that the results are also strongly model dependent. Once again the non-local forces predict more binding and, similarly, a reduced kinetic energy. The expectation values of H agree within the numerical accuracy of 50 keV with the BE’s E_α , which have been directly obtained from the YE’s.

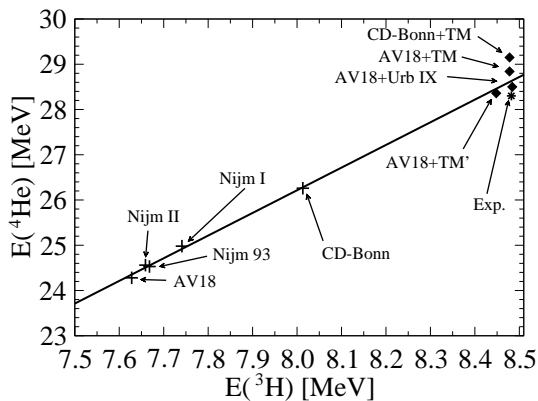


FIG. 3: Tjon-line: α particle binding-energy predictions $E(^4\text{He})$ dependent on the predictions for the ^3H binding energies for several realistic interaction models. Predictions of interaction models without (crosses) and with (diamonds) a 3NF are shown. The experimental point is marked by a star. The line represents a least square fit to the predictions of models without a 3NF.

interaction	E_α	H	T	V_{NN}	V_{3NF}
CD-Bonn+TM	-29.15	-29.09	83.92	-106.16	-6.854
AV18+TM	-28.84	-28.81	111.84	-132.62	-8.033
AV18+TM'	-28.36	-28.40	110.14	-133.36	-5.178
AV18+Urb-IX	-28.50	-28.53	113.21	-135.81	-5.929
AV18+Urb-IX (Argonne) [28]	-28.34(4)	—	110.7(7)	-135.3(7)	-6.3(1)
Exp.	-28.30	—	—	—	—

TABLE V: α particle binding-energy predictions E_α for the CD-Bonn and AV18 interactions in conjunction with various 3NF's, compared to the experimental value and the Argonne-Los Alamos result. The expectation values of the kinetic energy T , the NN interaction V_{NN} , the 3NF V_{3NF} and the Hamiltonian operator H are also shown. All energies are given in MeV.

In Ref. [71] an fascinating linear correlation of the α particle and ^3H BE's has been observed, known as the Tjon-line. Our new results confirm this correlation for the newest NN forces. This is displayed in Fig. 3. One sees that all predictions based on only NN forces are situated on a straight line. However, the experimental point slightly deviates from this line hinting to dynamical ingredients beyond the NN interaction and the non-relativistic Schrödinger equation. We also observe a strong dependence of this result on the accuracy of the NN force. Omitting the electromagnetic part of the AV18 NN interaction leads to 16 keV overbinding for the deuteron. A calculation based on this potential resulted in a visible deviation from the Tjon-line.

In the next step we also include 3NF's into our Hamiltonian. As discussed above, we adjusted these force in conjunction with the different NN interactions. We expect a much smaller dependence of the BE's on the 3N Hamiltonians in this case, because we remove in this way model dependences, which are correlated to the 3N BE. As one learns from the Tjon-line these are the dominant ones. Our results are given in Table V. Again we obtained an accuracy of the BE's E_α of 50 keV. The convergence is slower for these calculations. Therefore, we do not find the same accuracy for the expectation values as for the BE's. For these we estimate an error of 100 keV, which is still within 0.2 % of the kinetic energy.

For the NN and 3N forces used, we observe a small overbinding of 60 to 800 keV. These results are also included in Fig. 3. For the TM' and Urb-IX results we find only small deviations of our results from the Tjon-line. For TM we see more deviations. The TM force seems to destroy the correlation between the ^3H and α particle BE's. Though the TM' force and the Urb-IX interaction are quite different, their BE predictions seem to be comparable. Unfortunately the adjustment of the 3N force has not been done with the same accuracy for TM'. In view of the very expensive calculations necessary to improve the TM' results and in view of the expected agreement of the TM' and Urb-IX BE's, we did not re-calculate for TM', but omit its results in the following argumentation. The average BE for the α particle using only a NN interaction (based on the restricted choice shown in Table IV) is -24.9 MeV or 88 % of the α particle BE. Based on the TM and Urb-IX results in Table V, we estimate an average 3NF contribution to the α particle binding of 3.9 MeV or 14 % of the experimental BE. From the same results we find an average overbinding of 500 keV or 2 % of the BE. The contribution of the 3NF is strongly dependent on the NN interaction due to the adjustment of

interaction	$T = 0$	$T = 1$	$T = 2$
AV18	99.992	0.003	0.005

TABLE VI: Contribution of different total isospin states to the α particle wave function. The values are given in %.

these forces to the 3N BE. The model dependence of the overbinding is much smaller, but depends on the NN and the 3N force. One can consider this overbinding as the effect of a missing repulsive 4N force. The average size of this force can be expected to be 2 % of the BE in the α particle. Certainly the size of this force will be related to the NN and 3N forces used. The approach employed in [22] shows that these 4N forces are related to the 3N Hamiltonians in the same way as the 3N forces to the 2N Hamiltonians. We conclude from our results that we have found numerical evidence that 4N forces are, indeed, much smaller than 3N forces, at least in conjunction with today's NN and 3N interactions. We do not exclude that new additional 3NF terms could be found, which reduce the necessary contribution of 4N forces. The results support the generally accepted assumption that meaningful nuclear-structure calculations can be performed utilizing bare NN and 3N interactions in a microscopically self-consistent manner. We expect that 4N forces probably show up in heavier nuclei in the same order of magnitude (2 % of the BE). We, therefore, suggest to take an error of this size into account, when one discusses BE's for systems with $A > 4$, based on present NN and 3N forces.

C. Properties of the α particle WF

Besides the BE's, we are also interested in the WF of the 4N system, because it serves as input to several analyses of experiments involving the α particle. Most of these calculations are based on plane wave impulse approximation (PWIA). These calculations are directly sensitive to the WF. Model dependences of the WF are hints to model dependences of these observables. However, because WF's are not observable themselves, we emphasize that these dependences might disappear once the full dynamics are taken into account.

We start with a contribution of the different isospin states to the WF. Because we made a full, isospin breaking calculation for AV18 only, there is only one result shown in Table VI. The results for the 3N system do not depend on the interaction used [55]. Therefore, we do not expect model dependences here.

One sees an extremely small contribution of the $T = 1$ and $T = 2$ component to the WF. However, it is of interest that our $T = 1$ probability, based on realistic nuclear forces, is larger than the one estimated in [46]. There the $T = 1$ admixture has been found to be about $7 \cdot 10^{-4}$ % and the $T = 2$ state has not been considered. We found the $T = 2$ component nearly twice as large as the $T = 1$ admixture. Moreover the form of our $T = 1$ state will also be different from the one in [46]. As a consequence the isospin admixture correction to the asymmetry as given in [46] will change. A renewed evaluation of that correction, also including the larger $T = 2$ state has not been carried through, but appears interesting in view of ongoing experiments.

WF properties are also important for comparisons to other calculational schemes for treating the 4N system. Among the most simple of these properties are the S , P and D -wave probabilities of the WF. These are given in Table VII for the models based on the CD-Bonn and AV18 interactions. The values given in Table VII are based on overlaps between the YC's and the WF's, similar to those for the kinetic energies. These numbers are more accurate than the results given in [37]. However, the differences are not significant, as they affect only the last digit of the results.

As expected the orbital S -state is dominant. The D -state probability is sizable, very similar to results for ^3H [55], and the P -state gives only a small contribution. The D -state probability for 3N Hamiltonians, based on CD-Bonn, is smaller than those for models based on the AV18. This is related to the smaller tensor force of non-local interactions. It sticks out that all 3NF's lead to an increase of the P -wave probability by a factor of 2.

This raises the question, whether the considered 3NF really act differently in the 4N system. Because of the scarce knowledge on 3NF's, this issue is very important. It insures that we get insight into possible impacts of 3NF's in general, only if our models cover a wide range of interactions. To verify this issue, we decompose the WF's into parts with different total orbital angular momentum, namely S , P and D -states. Based on these components, we calculate the expectation values of the Urb-IX and TM 3NF's for three different WF's. One is based on the AV18 interaction only, one on the AV18+Urb-IX and the last on the AV18+TM. Four kinds of matrix elements dominate the total expectation value of the 3NF: the diagonal S - S -state and D - D -state matrix elements and the overlaps of S -state with P - and D -state. Table VIII shows our results. In the second and fourth columns expectation values for Urb-IX and TM are shown for the same WF, based on AV18. One observe a strong disagreement of these matrix elements. The diagonal elements for Urb-IX are strongly repulsive. They seem to be driven by the isospin and spin independent, phenomenological short-range core of the Urb-IX model. In strong contrast, the S - S matrix element contributes most

interaction	S	P	D
CD-Bonn	89.06	0.22	10.72
CD-Bonn+TM	89.65	0.45	9.90
AV18	85.87	0.35	13.78
AV18+TM	85.36	0.77	13.88
AV18+TM'	83.58	0.75	15.67
AV18+Urb-IX	83.23	0.75	16.03

TABLE VII: S , P and D state probabilities for the ^4He wave functions. All probabilities are in %.

3NF	Urb-IX		TM	
WF	AV18	AV18+Urb-IX	AV18	AV18+TM
S-S	3.16	2.74	-2.34	-4.09
S-P/P-S	-0.96	-2.10	-1.22	-3.56
S-D/D-S	-5.44	-7.46	2.08	-0.14
D-D	0.59	0.85	0.01	0.06

TABLE VIII: Contribution of different total orbital angular momenta in the wave functions to the expectation values of the Urb-IX and TM 3NF's. All energies are given in MeV.

of the attraction in the case of the TM. The attraction of Urb-IX is contributed by the S - D overlap. This is a major difference in the action of both models in the 4N system. It insures that we used, indeed, very different 3NF models though both are based on the 2π exchange mechanism. Additionally, we see in columns three and five of the table the expectation values based on WF's for the full Hamiltonian. These expectation values differ sizably from the ones based on the AV18 WF. We confirm for both 3NF's that a perturbative treatment of them is impossible. For the 3N system this was already emphasized in Refs. [72, 73, 74]. Especially interesting is the S - D overlap of the TM force. The AV18 WF result is strongly repulsive, whereas the full calculation leads to a slightly attractive contribution. This suggests interesting changes of the 3N configurations in the α particle due to this force.

Are these changes in the 3N configuration visible in momentum distributions? We start in Fig. 4 with a comparison of the nucleon momentum distribution

$$D(p) = \frac{1}{4\pi} \langle \Psi \ J = 0 \ M = 0 | \delta(p - q_4) | \Psi \ J = 0 \ M = 0 \rangle \quad (6)$$

for WF's based on different NN interactions. The momentum distributions are angular independent. We only consider the $T = 0$ components here. Therefore, the proton and neutron distributions are equal. Because we include in both calculations a 3NF, the WF's are the result of calculations, which roughly give the same BE's. This insures that we do not find differences, which can be traced back to a higher density of the nucleus. The distributions are equal for momenta below $p = 1 \text{ fm}^{-1}$ for both WF's. For momenta between $p = 1 \text{ fm}^{-1}$ and $p = 2 \text{ fm}^{-1}$ the deviations are moderate. Above this momentum the AV18 WF is much bigger. We find a clear difference between CD-Bonn and AV18 in this momentum region.

We do not see similar deviations comparing the momentum distributions for different 3NF's. This is shown in Fig. 5. The WF's shown there are based on the same NN interaction, AV18, but differ in the 3NF used. Again the BE's are comparable and there can be no deviations expected because of density differences. In fact one observes that the distributions are nearly equal for all models in the whole momentum range. This indicates a remarkable stability of momentum distributions with respect to the 3NF. This is in accord with the same independence of the 3NF choice for T , the second moment of the momentum distribution, as shown in Table V.

The correlations of two nucleons in nuclei are of great theoretical interest. Defined as the probability that two nucleons have a certain distance inside the nucleus, one finds very similar correlations for nuclei with different A [51, 75]. The correlation is characterized by the strong short-range repulsion of nuclear forces, leading to a small probability that two nucleons are close to each other. However, the quantitative results depend on the force model used. For the 3N system this has been shown in [9], and we find similar results for the 4N system [51]. These correlations are not observable. Therefore, difference in this WF property might not show up in observables. Electron induced scattering experiments, which intent to see these correlations also see effects of meson exchange currents (MEC's) and final state interactions (FSI's). Therefore a complete dynamical description of these processes is necessary [76].

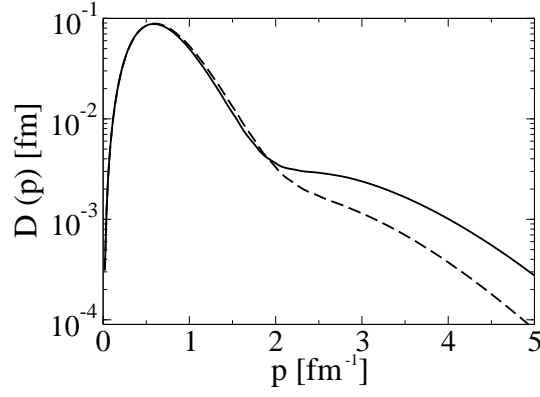


FIG. 4: Nucleon momentum distributions in ${}^4\text{He}$ on a logarithmic scale. The distribution functions are based on calculations using the AV18+TM (solid line) and CD-Bonn+TM (dashed line) potentials. The functions are normalized to $\int D(p)dp = \frac{1}{4\pi}$.

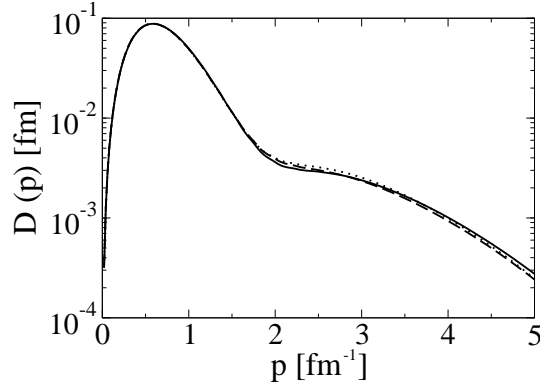


FIG. 5: Nucleon momentum distributions in ${}^4\text{He}$ on a logarithmic scale. The distribution functions are based on calculations using the AV18+TM (solid line), AV18+Urb-IX (dotted line) and AV18+TM' (dashed line) potentials. The functions are normalized to $\int D(p)dp = \frac{1}{4\pi}$.

Nevertheless, we want to show those correlations here. Two-nucleon knock-out experiments are expected to provide information on relative momentum distributions (see for instance [76, 77, 78]). In the PWIA these are sensitive to the distribution of relative momenta in the nucleus. Consequently, we show in the following momentum correlations, defined as

$$C^{SM_S}(\vec{p}) = \frac{p^2}{4\pi} \langle \Psi \ J=0 \ M=0 | \delta(\vec{p}_{12} - \vec{p}) | S \ M_S \rangle \langle S \ M_S | \Psi \ J=0 \ M=0 \rangle \quad (7)$$

They are the probabilities to find a pair of nucleons in a spin state $|S \ M_S \rangle$ and with a relative momentum \vec{p} . A similar definition in configuration space is given in Ref. [75], where it has been observed numerically that this function has a simple angular dependence, which can be expanded in two Legendre polynomials $P_f(\hat{p} \cdot \hat{e}_z)$ for $f=0$ and $f=2$:

$$C^{SM_S}(\vec{p}) = C_{f=0}^S(p) + C_{f=2}^{SM_S}(p) P_2(\hat{p} \cdot \hat{e}_z) \quad (8)$$

It only depends on the angle between the momentum and the quantization axis \hat{e}_z . In Appendix A we give an analytical proof of this relation.

The probability for two nucleons to be in a fixed spin state S is given by

$$N_S = \sum_{M_S} \langle \Psi \ J=0 \ M=0 | S \ M_S \rangle \langle S \ M_S | \Psi \ J=0 \ M=0 \rangle \quad (9)$$

For completeness these values are given in Table IX. In the following we will always normalize the correlations to $4\pi \int dp C(p) = 1$. The probabilities show the importance of individual channels to the total correlation.

interaction	$S = 0$	$S = 1$
CD-Bonn	44.60	55.40
CD-Bonn+TM	44.98	55.02
AV18	43.07	56.93
AV18+TM	42.95	57.05
AV18+TM'	42.05	57.95
AV18+Urb-IX	41.87	58.13

TABLE IX: Probabilities N_S to find NN pairs in spin $S = 0$ and $S = 1$ states in ${}^4\text{He}$ as given in Eq. (9). All probabilities are given in %.

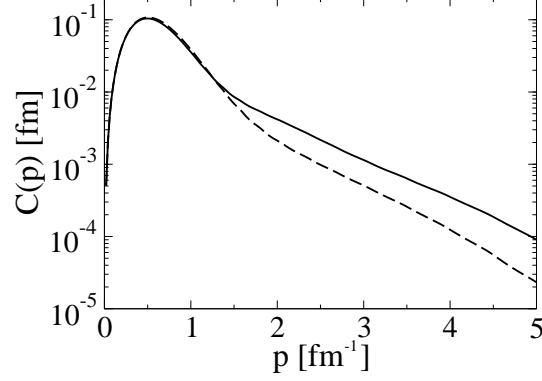


FIG. 6: Spin-averaged NN momentum correlations in ${}^4\text{He}$ for the AV18+TM (solid line) and the CD-Bonn+TM (dashed line) interactions. The functions are normalized to $\int C(p)dp = \frac{1}{4\pi}$.

In Figs. 6 and 7 spin independent momentum correlations are shown, which have been obtained by summing over all SM_S states. Obviously, because of no fixed quantization axis, they are angular independent. The first figure shows the momentum correlation for the CD-Bonn+TM and AV18+TM interactions. Similar to the distribution functions, they show discrepancies above $p = 1 \text{ fm}^{-1}$. In contrast, we did not find a similar model dependence for different 3NF forces. This is shown in Fig. 7 and suggests that 3NF models do not affect observables, which are considered to be sensitive to NN correlations. A search for kinematical regions, where FSI's and MEC's are suppressed, might reveal these correlations. In this case they should show up for momenta greater than $p = 1 \text{ fm}^{-1}$.

We also show the angular dependence of these momentum correlations. In Figs. 8 and 9 both parts of the correlation, as defined in Eq. (8), are displayed for $S = 1$ and $M_S = 0$. The angular dependent part does not depend on the 3NF,

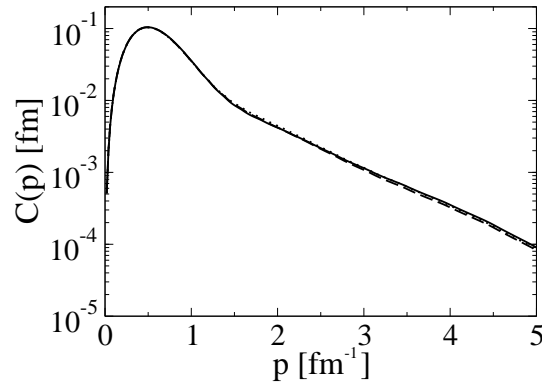


FIG. 7: Spin-averaged NN momentum correlations in ${}^4\text{He}$ for the AV18+TM (solid line), the AV18+Urb-IX (dotted line) and the AV18+TM' (dashed line) interactions. The functions are normalized to $\int C(p)dp = \frac{1}{4\pi}$.

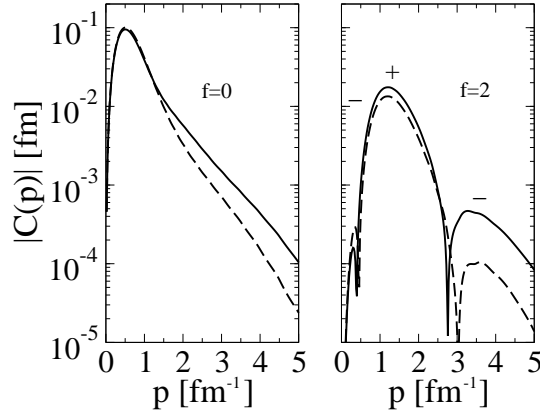


FIG. 8: Angular independent ($f = 0$) and dependent ($f = 2$) parts of the NN correlations $C^{S M_S}$ in ${}^4\text{He}$ for spin $S = 1$ and its third component $M_S = 0$, as defined in the text, compared for different interactions on a logarithmic scale. The correlation functions are based on calculations using the AV18+TM (solid lines) and CD-Bonn+TM (dashed lines) potentials. The functions are normalized, such that the angular independent part fulfills $\int dp C(p) = \frac{1}{4\pi}$. The magnitude $|C|$ is shown. $+$ ($-$) indicates positive (negative) $C_{f=2}$.

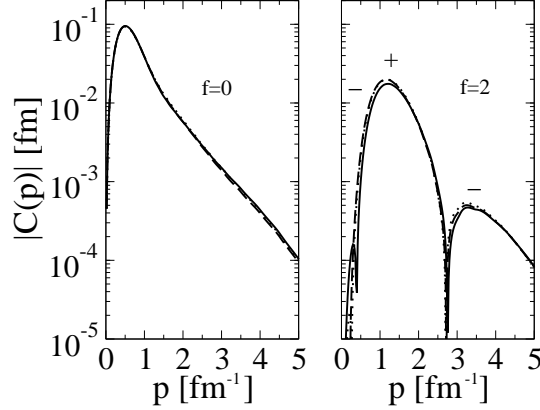


FIG. 9: Same as Fig. 8, except that the correlation functions are based on calculations using the AV18+TM (solid lines), AV18+Urb-IX (dotted lines) and AV18+TM' (dashed lines) potentials.

but for higher momenta, on the NN interaction. Around $p = 1 \text{ fm}^{-1}$ the $f = 2$ part is comparable in size to the $f = 0$ part. In this region one can expect a visible angular dependence of the correlation. This is related to the toroidal structures found in configuration space correlations in [75].

In recent years a knock-out reaction on ${}^4\text{He}$ with ${}^3\text{H}$ in the final state has received a great deal of attention [44, 79, 80, 81]. It has been shown that this reaction might be sensitive to the short-range correlations in nuclei [82]. A first experiment has not shown the expected dip in the cross section [79], which has been tracked back to effects of MEC's and FSI's. Ongoing experiments probe this reaction in different kinematical configurations, which are expected to be more sensitive to the correlations. The cross sections in the PWIA or in the more reliable Generalized Eikonal Approximation approach [83] are connected to the ${}^4\text{He}/{}^3\text{H}$ overlap functions

$$T(p) = \sum_{m_t} \langle \Psi J = 0 M = 0 | \delta(q_4 - p) | \phi_t j_t m_t \rangle \langle \phi_t j_t m_t | \Psi J = 0 M = 0 \rangle \quad (10)$$

The momentum of the fourth particle is fixed to p and the state of the other three is projected on the triton state ϕ_t with spin $j_t = \frac{1}{2}$ and third component m_t . Because of the sum over different orientations of the ${}^3\text{H}$ state, T is angular independent. One can show that this is still true, if one fixes m_t [51]. The probability to find a ${}^3\text{H}$ inside the α particle is given by $N_t = \int dp T(p)$. For completeness we give our results for N_t in Table X. The results depend slightly on the interaction model, but are of the order of 80 %. Thus, one observes a definite change in the 3N configuration in the presence of the fourth nucleon.

interaction	$N_t(^4\text{He})$
CD-Bonn	84.46
CD-Bonn +TM	83.49
AV18	82.40
AV18+TM	80.84
AV18+Urb-IX	80.33
AV18+TM'	80.54

TABLE X: Normalization constants N_t of the ^3H - p overlap distributions in ^4He . Results are given in %.

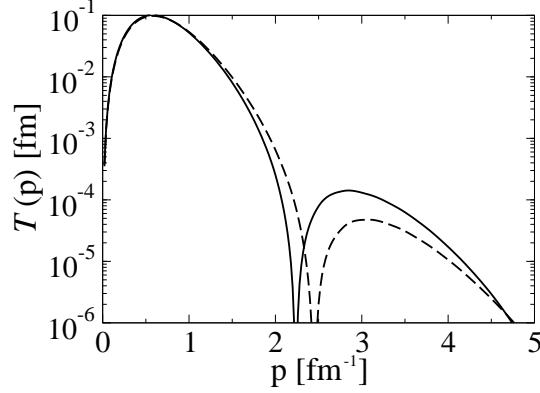


FIG. 10: ^3H - p momentum distribution T in ^4He on a logarithmic scale. The distribution functions are based on calculations using the AV18+TM (solid line) and CD-Bonn+TM (dashed line) potentials. The functions are normalized to $\int T(p)dp = \frac{1}{4\pi}$.

Fig. 10 shows the dependence of T on the NN interaction. The function exhibits a dip structure around $p = 2 \text{ fm}^{-1}$. The structure is the result of a node in the momentum space s -wave function of the fourth particle relative to the other three. This node is a necessary consequence of the short-range repulsion. Parity and angular momenta for ^3H and ^4He guarantee that only the s -wave contributes to T . The figure shows that T , indeed, depends on the NN interaction.

The comparison in Fig. 11 of the results for different 3NF's show that T does not depend on the 3NF's. Therefore, our results confirm that the measurement of T might be valuable to pin down the correlations of two nucleons due to different NN forces (if FSI and MEC effects would be negligible).

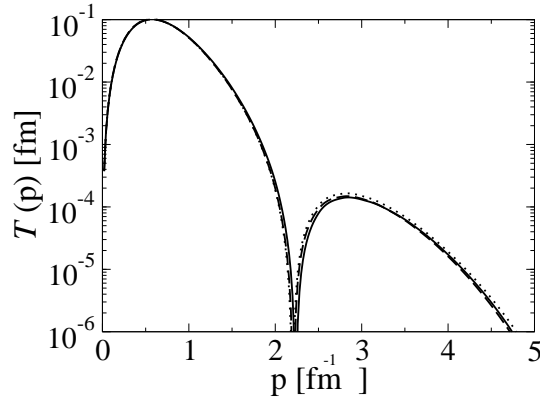


FIG. 11: Same as Fig. 10, except that the distribution functions are based on calculations using the AV18+TM (solid line), AV18+Urb-IX (dotted line) and AV18+TM' (dashed line) potentials.

IV. CONCLUSIONS AND OUTLOOK

We solved the Faddeev-Yakubovsky equations for the bound 4N system in momentum space and obtained converged results. Two-nucleon interactions, by themselves, underbind the α particle and leave room for considerable model dependences. Taking properly adjusted 3NF's into account, one can considerably reduce the model dependences of the BE's. The combinations of NN and 3N forces lead, in general, to a small overbinding, suggesting that 4N forces are repulsive and much smaller than 3N forces.

We also investigated model dependences of the WF. For momenta below $p = 1 \text{ fm}^{-1}$ we do not observe any model dependences in the momentum distributions and correlations. For higher momenta, only effects of the NN interaction show up, because the 3NF's do not affect these single nucleon and NN properties.

In contrast, we found a huge effect of 3N forces on 3N correlations visible in the matrix elements of the 3N force. These effects require further visualization in future studies. We also found that the α particle ground state is an extremely pure $T = 0$ isospin state. The admixtures of $T = 1$ and $T = 2$ states are of the order of 0.003 % and 0.005 %, respectively. This sharpens and questions the result found before in [46].

These calculations provide a baseline for the analysis of experiments involving the α particle, which require highly accurate WF's and insight into NN-force model dependences. The technical developments presented are also important for further studies of nuclear interactions based on χ PT. First studies have already been started [19, 21, 84]. χ PT allows a systematic derivation of 3NF's, which are consistent with the NN forces. An investigation of these 3N forces requires accurate techniques for solving the 3N and 4N Schrödinger equation, in order to fix the parameters of the force and to see their effects. The bound states are an interesting object for these studies, because they are the physical quantities very sensitive to 3NF effects and are dominated by the low-energy properties of the nuclear interaction.

Acknowledgments

A.N. and B.R.B. acknowledge partial support from NSF grant# PHY0070858. The numerical calculations have been performed on the Cray T3E of the NIC in Jülich, Germany.

APPENDIX A: PARTIAL WAVE DECOMPOSITION OF CORRELATION FUNCTIONS

The spin-dependent correlation functions are angular dependent. In momentum space and for a general nuclear A -body bound-state Ψ with angular momentum J M , it is defined as

$$C^{SM_S}(\vec{p}) = \frac{p^2}{4\pi} \sum_M \langle \Psi J M | \delta(\vec{p}_{12} - \vec{p}) | S M_S \rangle \langle S M_S | \Psi J M \rangle \quad (\text{A1})$$

The operator $\delta(\vec{p}_{12} - \vec{p}) | S M_S \rangle \langle S M_S |$ acts only on the subsystem of particles 1 and 2, i.e., (12). Therefore we choose coordinates, which single out this subsystem and denote the coordinates of the remaining particles by $\alpha_{A-2} J_{A-2} M_{A-2}$, where we have separated the angular momentum quantum numbers. α_{A-2} also includes the motion of the (12) subsystem relative to the $A - 2$ spectators. The two-body subsystem is described by the usual momentum p_{12} and quantum numbers l_{12} , s_{12} and j_{12} and the third component m_j . Resolving the coupling of the angular momentum of the (12) subsystem and the spectators to the total angular momentum, one obtains for the correlation

$$\begin{aligned} C^{S M_S}(\vec{p}) = & \frac{1}{2J+1} \sum_M \sum_{\alpha_{A-2}} \sum_{\substack{l_{12}l'_{12}s_{12}s'_{12} \\ J_{A-2}M_{A-2} j_{12}j'_{12}m_jm'_j}} \int dp_{12} p_{12}^2 \int dp'_{12} p_{12}'^2 \\ & (j_{12}J_{A-2}J, m_jM_{A-2}M) (j'_{12}J_{A-2}J, m'_jM_{A-2}M) \\ & \langle \Psi JM | p_{12} \alpha_{A-2} ((l_{12}s_{12})j_{12}J_{A-2})JM \rangle \langle p'_{12} \alpha_{A-2} ((l'_{12}s'_{12})j'_{12}J_{A-2})JM | \Psi JM \rangle \\ & \langle p_{12}(l_{12}s_{12})j_{12}m_j | \delta^3(\vec{p} - \vec{p}_{12}) | S M_S \rangle \langle S M_S | p'_{12}(l'_{12}s'_{12})j'_{12}m'_j \rangle \end{aligned} \quad (\text{A2})$$

The nuclear bound state WF $\langle p'_{12} \alpha_{A-2} ((l'_{12}s'_{12})j'_{12}J_{A-2})JM | \Psi JM \rangle$ is independent of M . We choose $M = J$ in these matrix elements and perform the M and M_{A-2} summation, using the orthogonality relations for the Clebsch-

Gordan coefficients. This leads to

$$\begin{aligned}
C^{S M_S}(\vec{p}) &= \sum_{\alpha_{A-2} J_{A-2}} \sum_{\substack{l_{12} s_{12} j_{12} \\ l'_{12} s'_{12}}} \int dp_{12} p_{12}^2 \int dp'_{12} p_{12}'^2 \\
&\quad \frac{1}{2j_{12} + 1} \sum_{m_j} \langle p_{12}(l_{12} s_{12}) j_{12} m_j | \delta^3(\vec{p} - \vec{p}_{12}) | S M_S \rangle \langle S M_S | p'_{12}(l'_{12} s'_{12}) j_{12} m_j \rangle \\
&\quad \langle \Psi J J | p_{12} \alpha_{A-2} ((l_{12} s_{12}) j_{12} J_{A-2}) J J \rangle \langle p'_{12} \alpha_{A-2} ((l'_{12} s'_{12}) j_{12} J_{A-2}) J J | \Psi J J \rangle
\end{aligned} \tag{A3}$$

In this form the problem is reduced for arbitrary nuclei to the matrix element

$$M_{12} \equiv \frac{1}{2j_{12} + 1} \sum_{m_j} \langle p_{12}(l_{12} s_{12}) j_{12} m_j | \delta^3(\vec{p} - \vec{p}_{12}) | S M_S \rangle \langle S M_S | p'_{12}(l'_{12} s'_{12}) j_{12} m_j \rangle, \tag{A4}$$

which is diagonal in j_{12} and m_j .

By inserting the unity operator in states of 3D momentum and resolving the coupling of spins and orbital angular momenta, we are able to simplify the expression to

$$\begin{aligned}
M_{12} &= \delta_{s_{12} s'_{12}} \delta_{s_{12} S} \frac{\delta(p_{12} - p)}{p_{12} p} \frac{\delta(p'_{12} - p)}{p'_{12} p} \frac{1}{2j_{12} + 1} \sum_{m_j} \\
&\quad (l_{12} S j_{12}, m_j - M_S M_S) (l'_{12} S j_{12}, m_j - M_S M_S) Y_{l_{12} m_j - M_S}^*(\hat{p}) Y_{l'_{12} m_j - M_S}(\hat{p})
\end{aligned} \tag{A5}$$

Using standard techniques, one can recouple the angular momenta to obtain a coupled spherical harmonic $\mathcal{Y}_{l_{12} l'_{12}}^{f \mu}(\hat{p} \hat{p})$. It turns out that only $\mu = 0$ contributes, which is expected, because fixing the spin only fixes the z -axis. The matrix elements depend only on $x = \hat{p} \cdot \hat{e}_z$. This dependence can be expanded in Legendre polynomials and one ends up with

$$\begin{aligned}
M_{12} &= \delta_{s_{12} s'_{12}} \delta_{s_{12} S} \frac{\delta(p_{12} - p)}{p_{12} p} \frac{\delta(p'_{12} - p)}{p'_{12} p} \sum_f (-)^{S-j_{12}} (-)^{l_{12}+l'_{12}-f} \sqrt{\frac{(2l_{12}+1)(2l'_{12}+1)(2f+1)}{2S+1}} \\
&\quad \left\{ \begin{matrix} S & l_{12} & j_{12} \\ l'_{12} & S & f \end{matrix} \right\} (S f S, M_S 0) (l_{12} l'_{12} f, 00) \frac{1}{4\pi} P_f(x)
\end{aligned} \tag{A6}$$

Because S is restricted to 0 and 1, the order of the Legendre polynomial f can only take the values 0, 1 and 2. Parity conservation fixes the phase $(-)^{l_{12}+l'_{12}} = 1$. Therefore, the Clebsch-Gordan coefficient $(l_{12} l'_{12} f, 00)$ demands even f 's. Because of this, the expansion of the angular dependence contains only two Legendre polynomials: $P_0(x)$ and $P_2(x)$. This proves the form of Eq. (8). From the explicit form of M_{12} one also reads off that the M_S dependence is given by an overall Clebsch-Gordan coefficient. This justifies the fact that we only present results for $M_S = 0$ in Section III C. We also see that the $f = 0$ part of C is independent of M_S . Finally, we would like to note that the expressions are also valid in configuration space, replacing the momenta by the corresponding distances.

APPENDIX B: TREATMENT OF THE 3NF EMBEDDED IN THE 4N HILBERT SPACE

1. TM-like forces

We consider the 3NF as the successive applications of NN-like interactions, which, however, do not respect parity and rotational invariance. Only the full 3NF respects these symmetries [50]. The YE's 2 and 3 require the matrix elements

$$\langle (12)3, 4 | V_{123}^{(3)} | \Psi \rangle \tag{B1}$$

where we can assume that the state Ψ is antisymmetric in the nucleons 123.

	$4(2\pi)^6 V_0 [m_N^{-2}]$	a $[m_\pi^{-1}]$	b $[m_\pi^{-3}]$	c $[m_\pi^{-3}]$	d $[m_\pi^{-3}]$
TM	179.7	1.13	-2.58	1.00	-0.753
TM'	179.7	-0.87	-2.58	0.00	-0.753

TABLE XI: Strength constants of the TM [23] and TM' [50] 3NF's. The numbers are in units of the nucleon mass $m_N = 938.926$ MeV and the π mass $m_\pi = 139.6$ MeV.

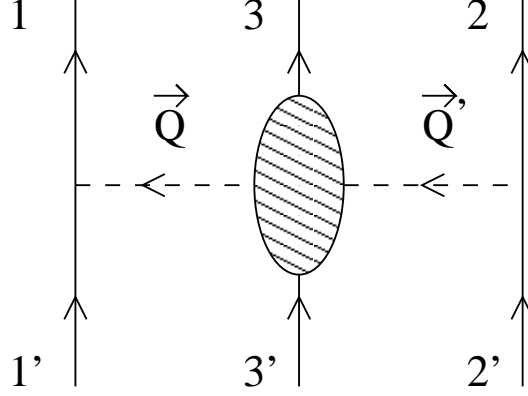


FIG. 12: Symbolic representation of a 3NF, like the TM force, and the definition of the momentum transfers \vec{Q} and \vec{Q}' within the two subsystems

One distinguishes four terms in the TM force, the so called a -, b -, c - and d -term, which are given by their individual strength constants. These constants are listed together with V_0 in Table XI.

$$V_{123}^{(3)} = V_0 \left(a \vec{\tau}_1 \cdot \vec{\tau}_2 W_{23}^a W_{31}^a + b \vec{\tau}_1 \cdot \vec{\tau}_2 \vec{W}_{23}^b \cdot \vec{W}_{31}^b + c \vec{\tau}_1 \cdot \vec{\tau}_2 (W_{23}^c W_{31}^c + W_{23}^c W_{31}^a) + d \vec{\tau}_3 \cdot \vec{\tau}_1 \times \vec{\tau}_2 \vec{W}_{23}^d \cdot \vec{W}_{31}^b \right) \quad (\text{B2})$$

where we have separated the isospin operators (Pauli isospin matrices τ_i) and the spin-orbital operators W .

The W 's can be read off from the definition of the TM force in momentum space, as given in Ref. [50].

$$\begin{aligned} W_{23}^a &= F(\vec{Q}'^2) \frac{\vec{\sigma}_2 \cdot \vec{Q}'}{\vec{Q}'^2 + m_\pi^2} & W_{31}^a &= F(\vec{Q}^2) \frac{\vec{\sigma}_1 \cdot \vec{Q}}{\vec{Q}^2 + m_\pi^2} \\ \vec{W}_{23}^b &= F(\vec{Q}'^2) \frac{\vec{\sigma}_2 \cdot \vec{Q}'}{\vec{Q}'^2 + m_\pi^2} \vec{Q}' & \vec{W}_{31}^b &= F(\vec{Q}^2) \frac{\vec{\sigma}_1 \cdot \vec{Q}}{\vec{Q}^2 + m_\pi^2} \vec{Q} \\ W_{23}^c &= F(\vec{Q}'^2) \frac{\vec{\sigma}_2 \cdot \vec{Q}'}{\vec{Q}'^2 + m_\pi^2} \vec{Q}'^2 & W_{31}^c &= F(\vec{Q}^2) \frac{\vec{\sigma}_1 \cdot \vec{Q}}{\vec{Q}^2 + m_\pi^2} \vec{Q}^2 \\ \vec{W}_{23}^d &= F(\vec{Q}'^2) \frac{\vec{\sigma}_2 \cdot \vec{Q}'}{\vec{Q}'^2 + m_\pi^2} \vec{\sigma}_3 \times \vec{Q}' \end{aligned} \quad (\text{B3})$$

with the momentum transfers $\vec{Q} = \vec{k}_1 - \vec{k}_1'$ and $\vec{Q}' = \vec{k}_2' - \vec{k}_2$, as indicated in Fig. 12. The σ_i 's are Pauli spin matrices and the form factors are chosen to be $F(\vec{Q}^2) = \frac{\Lambda^2 - m_\pi^2}{\Lambda^2 + \vec{Q}^2}$.

Applied to a state vector ψ , all four terms have the form

$$\psi' \sim W_{23} I W_{31} \Psi, \quad (\text{B4})$$

where we have abbreviated the isospin operators by I .

By introducing the unit operator in the coordinates, which are natural for the W potentials, we are able to turn Eq. (B4) into

$$\langle (12)3, 4 | \psi' \rangle \sim \langle (12)3, 4 | (23)1, 4' \rangle \langle (23)1, 4' | W_{23} | (23)1, 4'' \rangle$$

$$< (23)1, 4'' | I | (31)2, 4''' > < (31)2, 4''' | W_{31} | (31)2, 4^* > < (31)2, 4^* | \Psi > . \quad (\text{B5})$$

We omit the integrals and sums over momenta and quantum numbers of the intermediate states, in order to simplify the expressions and denote by $(ij)k, l$ Jacobi coordinates, which single out the pair ij , the 3-body cluster ijk and the spectator l . Ψ originally enters in $(12)3, 4$ coordinates. But because of the antisymmetry of Ψ in the (123) subsystem, the $(31)2, 4$ coordinates are equivalent in this case.

Because the W_{23} 's do not respect the symmetries of nuclear interactions, the sum over $''$ - and $'''$ -states have to include other parities or other total angular momenta, depending on whether a/c of b/d -terms are considered. The $''$ -, $'''$ - and $'''$ -sums have also to include unphysical symmetric states of the (31) or (23) subsystems. The matrix elements of the coordinate transformations $< (23)1, 4'' | I | (31)2, 4''' >$ are given in Ref. [48, 51]. The isospin operator leads to a change of the isospin part of the transformation. The new isospin matrix elements have been derived in Ref. [50] for the 3N system and are given below for the 4N system for completeness.

The matrix elements for the different W 's are summarized below. For the a -term one finds

$$\begin{aligned} & < (31)2, 4 | W_{31}^a | (31)2, 4' > \\ &= \frac{\delta(q_4 - q'_4)}{q_4 q'_4} \frac{\delta(p_2 - p'_2)}{p_2 p'_2} \delta_{I_4 I'_4} \delta_{I_2 I'_2} \delta_{l_4 l'_4} \delta_{l_2 l'_2} \delta_{JJ'} \delta_{MM'} \delta_{j_3 j'_3} \delta_{j_{31} j'_{31}} \delta_{|l_{31} - l'_{31}|, 1} \\ & \quad 2\pi\sqrt{6} (-)^{j_{31}+1+\max(l_{31}, l'_{31})} \sqrt{\hat{s}_{31} \hat{s}'_{31}} \begin{Bmatrix} \frac{1}{2} & \frac{1}{2} & s'_{31} \\ 1 & s_{31} & \frac{1}{2} \end{Bmatrix} \begin{Bmatrix} l'_{31} & s'_{31} & j'_{31} \\ s_{31} & l_{31} & 1 \end{Bmatrix} \\ & \quad \sqrt{\max(l_{31}, l'_{31})} (p_{31} H_{l'_{31}}(p_{31}, p'_{31}) - p'_{31} H_{l_{31}}(p_{31}, p'_{31})) \end{aligned} \quad (\text{B6})$$

The operator has no isospin dependence; therefore, it is diagonal in isospin space. The momentum dependence is given in terms of the function H , which is a combination of Legendre polynomials of the second kind Q_l and their derivatives Q'_l .

$$H_l(p, p') = \frac{1}{pp'} (Q_l(B_{m_\pi}) - Q_l(B_\Lambda)) + \frac{\Lambda^2 - m_\pi^2}{2(pp')^2} Q'_l(B_\Lambda) \quad (\text{B7})$$

with $B_{m_\pi} = \frac{p^2 + p'^2 + m_\pi^2}{2pp'}$ and $B_\Lambda = \frac{p^2 + p'^2 + \Lambda^2}{2pp'}$.

The c -term looks very similar as the a -term and follows, if one replaces H in Eq. (B6) by

$$\tilde{H}_l(p, p') = -\frac{m_\pi^2}{pp'} (Q_l(B_{m_\pi}) - Q_l(B_\Lambda)) - \frac{\Lambda^2 - m_\pi^2}{2(pp')^2} \Lambda^2 Q'_l(B_\Lambda). \quad (\text{B8})$$

For our convenience, we used the abbreviation $\hat{k} = 2k + 1$ in these expressions. The notation of the different quantum numbers is an obvious generalization of the notation in Fig. 1.

Because the W_{23} - and W_{31} -operators are equivalent up to a renumbering of the particles, the matrix elements are equal up to a phase factor

$$< (23)1, 4 | W_{23}^{a,c} | (23)1, 4' > = (-)^{l_{31}+s_{31}+t_{31}+l'_{31}+s'_{31}+t'_{31}+1} < (31)2, 4 | W_{31}^{a,c} | (31)2, 4' > . \quad (\text{B9})$$

As we already mentioned, we replace the simple isospin transformation matrix element by a combination of the transformation and the isospin operator

$$< (23)1, 4 | \vec{\tau}_1 \cdot \vec{\tau}_2 | (31)2, 4' > = \delta_{TT'} \delta_{M_T M'_T} \delta_{\tau\tau'} (-6) (-)^{t_{23}} \sqrt{\hat{t}_{23} \hat{t}'_{31}} \begin{Bmatrix} \frac{1}{2} & \frac{1}{2} & t'_{31} \\ \frac{1}{2} & 1 & \frac{1}{2} \\ t_{23} & \frac{1}{2} & \tau \end{Bmatrix}. \quad (\text{B10})$$

The b - and d -terms are a slightly more complicated, because the NN-like potentials are now vector operators. The matrix elements of the spherical components $W^1 = -\frac{1}{\sqrt{2}} (W^x + iW^y)$, $W^0 = W^z$ and $W^{-1} = \frac{1}{\sqrt{2}} (W^x - iW^y)$ decompose into a Clebsch-Gordan coefficient and a reduced matrix element

$$< (31)2, 4 | W_{31}^\mu | (31)2, 4' > = (J'1J, M'\mu M) < (31)2, 4 | W_{31} | (31)2, 4' > . \quad (\text{B11})$$

The scalar product in spherical coordinates reads

$$\vec{W}_{23} \cdot \vec{W}_{31} = \sum_{\mu} (-)^{\mu} W_{23}^{\mu} W_{31}^{-\mu}. \quad (\text{B12})$$

Because there is no dependence on the third component of the total angular momentum, neither in the transformation matrix elements nor in the incoming state, we can analytically perform the M'' and μ -summations

$$\sum_{M''\mu} (-)^\mu (J''1J', M''\mu M') (J^*1J'', M^* - \mu M'') = \delta_{J'J^*} \delta_{M'M^*} \sqrt{\frac{\hat{J}''}{\hat{J}'}} (-)^{J''-J'} \quad (\text{B13})$$

and recover the conservation of the total angular momentum. The NN-like potentials effectively requires only the application of the reduced matrix elements and the additional factor $\sqrt{\frac{\hat{J}''}{\hat{J}'}} (-)^{J''-J'}$. The intermediate states are also M independent.

The generalization of the formulas given in Ref. [50] to the four-nucleon system yields

$$\begin{aligned} & \langle (31)2, 4 || W_{31}^b || (31)2, 4 \rangle' \\ &= \frac{\delta(q_4 - q'_4)}{q_4 q'_4} \frac{\delta(p_2 - p'_2)}{p_2 p'_2} \delta_{I_4 I'_4} \delta_{I_2 I'_2} \delta_{l_4 l'_4} \delta_{l_2 l'_2} (-)^{J'+J'_3+j_3+I_4+I_2+s_{31}+s'_{31}} \sqrt{\hat{J}' \hat{J}'_3 \hat{J}'_3 \hat{s}'_{31} \hat{s}_{31} \hat{J}'_{31} \hat{J}_{31}} \\ & \quad \left\{ \begin{matrix} j'_3 & 1 & j_3 \\ J & I_4 & J' \end{matrix} \right\} \left\{ \begin{matrix} 1 & j_{31} & j'_{31} \\ I_2 & j'_3 & j_3 \end{matrix} \right\} \left\{ \begin{matrix} \frac{1}{2} & \frac{1}{2} & s_{31} \\ 1 & s'_{31} & \frac{1}{2} \end{matrix} \right\} \\ & \quad \times \left[\delta_{l_{31} l'_{31}} \frac{2\pi}{3} \sqrt{6} (-)^{l_{31}+1} \left\{ \begin{matrix} j'_{31} & j_{31} & 1 \\ s_{31} & s'_{31} & l_{31} \end{matrix} \right\} \tilde{H}_{l_{31}}(p_{31} p'_{31}) \right. \\ & \quad \left. - 40\pi \sqrt{6} (-)^{s'_{31}+j_{31}} \left\{ \begin{matrix} 2 & 1 & 1 \\ l_{31} & s_{31} & j_{31} \\ l'_{31} & s'_{31} & j'_{31} \end{matrix} \right\} \sum_{\bar{l}} \hat{l} H_{\bar{l}}(p_{31} p'_{31}) \right. \\ & \quad \left. \times \sum_{a+b=2} \frac{p'_{31}{}^a p_{31}{}^b}{\sqrt{(2a)!(2b)!}} \left\{ \begin{matrix} b & a & 2 \\ l'_{31} & l_{31} & \bar{l} \end{matrix} \right\} (a \bar{l} l'_{31}, 00) (b \bar{l} l_{31}, 00) \right] \quad (\text{B14}) \end{aligned}$$

and

$$\begin{aligned} & \langle (23)1, 4 || W_{23}^d || (23)1, 4 \rangle' \\ &= \frac{\delta(q_4 - q'_4)}{q_4 q'_4} \frac{\delta(p_1 - p'_1)}{p_1 p'_1} \delta_{I_4 I'_4} \delta_{I_1 I'_1} \delta_{l_4 l'_4} \delta_{l_1 l'_1} (-)^{J'+J'_3+j_3+I_4+I_1+s_{23}+s'_{23}+1} \sqrt{\hat{J}' \hat{J}'_3 \hat{J}'_3 \hat{s}'_{23} \hat{s}_{23} \hat{J}'_{23} \hat{J}_{23}} \\ & \quad \left\{ \begin{matrix} j'_3 & 1 & j_3 \\ J & I_4 & J' \end{matrix} \right\} \left\{ \begin{matrix} 1 & j_{23} & j'_{23} \\ I_1 & j'_3 & j_3 \end{matrix} \right\} \\ & \quad \times \left[\delta_{l_{23} l'_{23}} i 4\pi \sqrt{6} (-)^{l_{23}+s_{23}} \left\{ \begin{matrix} l_{23} & s_{23} & j_{23} \\ 1 & j'_{23} & s'_{23} \end{matrix} \right\} \left\{ \begin{matrix} 1 & 1 & 1 \\ \frac{1}{2} & \frac{1}{2} & s'_{23} \\ \frac{1}{2} & \frac{1}{2} & s_{23} \end{matrix} \right\} \tilde{H}_{l_{23}}(p_{23} p'_{23}) \right. \\ & \quad \left. + i 240\pi \sqrt{6} (-)^{j'_{23}} \sum_{\chi} (-)^\chi \hat{\chi} \left\{ \begin{matrix} 2 & \chi & 1 \\ 1 & 1 & 1 \end{matrix} \right\} \left\{ \begin{matrix} 2 & \chi & 1 \\ l'_{23} & s'_{23} & j'_{23} \\ l_{23} & s_{23} & j_{23} \end{matrix} \right\} \left\{ \begin{matrix} 1 & 1 & \chi \\ \frac{1}{2} & \frac{1}{2} & s'_{23} \\ \frac{1}{2} & \frac{1}{2} & s_{23} \end{matrix} \right\} \right. \\ & \quad \left. \times \sum_{\bar{l}} \hat{l} H_{\bar{l}}(p_{23} p'_{23}) \sum_{a+b=2} \frac{p'_{23}{}^a p_{23}{}^b}{\sqrt{(2a)!(2b)!}} \left\{ \begin{matrix} b & a & 2 \\ l'_{23} & l_{23} & \bar{l} \end{matrix} \right\} (a \bar{l} l'_{23}, 00) (b \bar{l} l_{23}, 00) \right]. \quad (\text{B15}) \end{aligned}$$

The momentum dependent functions H and \tilde{H} are given in Eqs. (B7) and (B8).

Again, there is a simple phase relation between W_{23}^b and W_{31}^b

$$\langle (23)1, 4 | W_{23}^{b,d} | (23)1, 4' \rangle = (-)^{l_{31}+s_{31}+t_{31}+l'_{31}+s'_{31}+t'_{31}} \langle (31)2, 4 | W_{31}^{b,d} | (31)2, 4' \rangle \quad (\text{B16})$$

The isospin matrix element of the d -term differs from the one for the a -, b - and c -term, given in Eq. (B10). It reads

$$\begin{aligned} \langle (23)1, 4 | \vec{\tau}_3 \cdot (\vec{\tau}_1 \times \vec{\tau}_3) | (31)2, 4' \rangle &= \delta_{TT'} \delta_{M_T M'_T} \delta_{\tau\tau'} 24i (-)^{2\tau} \sqrt{\hat{t}_{23} \hat{t}'_{31}} \\ & \quad \sum_{\lambda} (-)^{3\lambda+\frac{1}{2}} \left\{ \begin{matrix} \lambda & \frac{1}{2} & 1 \\ \frac{1}{2} & \frac{1}{2} & t_{23} \end{matrix} \right\} \left\{ \begin{matrix} \tau & \frac{1}{2} & t_{23} \\ \frac{1}{2} & 1 & \lambda \\ t'_{31} & \frac{1}{2} & \frac{1}{2} \end{matrix} \right\}. \quad (\text{B17}) \end{aligned}$$

2. Urbana type forces

The functional form of the Urbana 3NF is much simpler. One usually expresses the Urbana interaction in terms of commutator and anticommutator parts. This reads

$$V_{123}^{(3)} = A_{2\pi} [\{X_{23}, X_{31}\} \{ \vec{\tau}_2 \cdot \vec{\tau}_3, \vec{\tau}_3 \cdot \vec{\tau}_1 \} + \frac{1}{4} [X_{23}, X_{31}] [\vec{\tau}_2 \cdot \vec{\tau}_3, \vec{\tau}_3 \cdot \vec{\tau}_1]] + U_0 T_\pi^2(r_{23}) T_\pi^2(r_{31}) \quad (\text{B18})$$

The force is explicitly defined in terms of NN interactions

$$X_{ij} = Y_\pi(r_{ij}) \vec{\sigma}_i \cdot \vec{\sigma}_j + T_\pi(r_{ij}) S_{ij} \quad (\text{B19})$$

X_{ij} is derived from the π exchange NN force. Therefore, it has a spin-spin part $\vec{\sigma}_i \cdot \vec{\sigma}_j$ and a tensor part

$$S_{ij} = 3 \vec{\sigma}_i \cdot \hat{r}_i \vec{\sigma}_j \cdot \hat{r}_j - \vec{\sigma}_i \cdot \vec{\sigma}_j. \quad (\text{B20})$$

The radial dependence is given as

$$Y_\pi(r) = \frac{e^{-m_\pi r}}{m_\pi r} (1 - e^{-cr^2})$$

$$T_\pi(r) = \left[1 + \frac{3}{m_\pi r} + \frac{3}{(m_\pi r)^2} \right] \frac{e^{-m_\pi r}}{m_\pi r} (1 - e^{-cr^2})^2 \quad (\text{B21})$$

The parameters $A_{2\pi}$, U_0 and c for the Urb-IX are given in Ref. [24].

In [5] it is shown that the application of the Urbana force can be rewritten as

$$\begin{aligned} < (12)3, 4 | \psi' > = 2A_{2\pi} < (12)3, 4 | (23)1, 4' > < (23)1, 4' | X_{23} | (23)1, 4'' > \\ & < (23)1, 4'' | I^- | (31)2, 4''' > < (31)2, 4''' | X_{31} | (31)2, 4^* > < (31)2, 4^* | \psi > \\ & + U_0 < (12)3, 4 | (23)1, 4' > < (23)1, 4' | T_\pi^2(r_{23}) | (23)1, 4'' > \\ & < (23)1, 4'' | (31)2, 4''' > < (31)2, 4''' | T_\pi^2(r_{31}) | (31)2, 4^* > < (31)2, 4^* | \psi > . \end{aligned} \quad (\text{B22})$$

The isospin operators are very similar to the ones encountered in the TM force

$$I^- \equiv 2(\vec{\tau}_1 \cdot \vec{\tau}_2 - \frac{i}{4} \vec{\tau}_3 \cdot \vec{\tau}_1 \times \vec{\tau}_2)$$

$$I^+ \equiv 2(\vec{\tau}_1 \cdot \vec{\tau}_2 + \frac{i}{4} \vec{\tau}_3 \cdot \vec{\tau}_1 \times \vec{\tau}_2). \quad (\text{B23})$$

It is easy to combine Eqs. (B10) and (B17) to find their matrix elements.

The matrix elements of the NN-like interactions X_{31} and $T_\pi^2(r_{31})$ read in momentum space

$$\begin{aligned} < (31)2, 4 | X_{31} | (31)2, 4' > \\ = & \frac{\delta(q_4 - q'_4)}{q_4 q'_4} \frac{\delta(p_2 - p'_2)}{p_2 p'_2} \delta_{I_4 I'_4} \delta_{I_2 I'_2} \delta_{l_4 l'_4} \delta_{l_2 l'_2} \delta_{JJ'} \delta_{MM'} \delta_{j_{31} j'_{31}} \\ & \left[\tilde{Y}_{l_{31}}(p_{31}, p'_{31}) \delta_{l_{31} l'_{31}} \delta_{s_{31} s'_{31}} (-3 + 4s_{31}) + \tilde{T}_{l_{31} l'_{31}}(p_{31}, p'_{31}) \delta_{s_{31} s'_{31}} \delta_{s_{31} 1} S_{l_{31} l'_{31} j_{31}} \right] \end{aligned} \quad (\text{B24})$$

and

$$\begin{aligned} < (31)2, 4 | T_\pi^2(r_{31}) | (31)2, 4' > \\ = & \frac{\delta(q_4 - q'_4)}{q_4 q'_4} \frac{\delta(p_2 - p'_2)}{p_2 p'_2} \delta_{I_4 I'_4} \delta_{I_2 I'_2} \delta_{l_4 l'_4} \delta_{l_2 l'_2} \delta_{JJ'} \delta_{MM'} \delta_{j_{31} j'_{31}} \delta_{l_{31} l'_{31}} \delta_{s_{31} s'_{31}} \bar{T}_{l_{31}}(p_{31}, p'_{31}). \end{aligned} \quad (\text{B25})$$

Here the tensor operator can be expressed in simple rational functions of the quantum numbers

$$S_{l_{31} l'_{31} j_{31}} = \begin{matrix} l_{31} = j_{31} - 1 \\ l_{31} = j_{31} \\ l_{31} = j_{31} + 1 \end{matrix} \begin{bmatrix} -2 \frac{j_{31}-1}{2j_{31}+1} & 0 & 6 \frac{\sqrt{j_{31}(j_{31}+1)}}{2j_{31}+1} \\ 0 & 2 & 0 \\ 6 \frac{\sqrt{j_{31}(j_{31}+1)}}{2j_{31}+1} & 0 & -2 \frac{j_{31}+2}{2j_{31}+1} \end{bmatrix} \quad (\text{B26})$$

$$l'_{31} = j_{31} - 1 \quad l'_{31} = j_{31} \quad l'_{31} = j_{31} + 1$$

We numerically perform the Fourier transformations

$$\begin{aligned}
\tilde{Y}_{l_{31}}(p_{31}, p'_{31}) &= \frac{2}{\pi} \int_0^\infty dr r^2 j_{l_{31}}(p_{31}r) Y_\pi(r) j_{l_{31}}(p'_{31}r) \\
\tilde{T}_{l_{31}l'_{31}}(p_{31}, p'_{31}) &= (-)^{l_{31}-l'_{31}} \frac{2}{\pi} \int_0^\infty dr r^2 j_{l_{31}}(p_{31}r) T_\pi(r) j_{l'_{31}}(p'_{31}r) \\
\bar{T}_{l_{31}}(p_{31}, p'_{31}) &= \frac{2}{\pi} \int_0^\infty dr r^2 j_{l_{31}}(p_{31}r) T_\pi^2(r) j_{l_{31}}(p'_{31}r)
\end{aligned} \tag{B27}$$

with the usual spherical Bessel functions $j_l(x)$.

Because these NN-like interactions are all symmetric with respect to an interchange of the subsystem particles, the matrix elements for the X_{23} and $T^2(r_{23})$ equal those for X_{31} and $T^2(r_{31})$, respectively

-
- [1] R. Machleidt, F. Sammarruca, and Y. Song, Phys. Rev. C **53**, R1483 (1996).
 - [2] R.B. Wiringa, V.G.J. Stoks, and R. Schiavilla, Phys. Rev. C **51**, 38 (1995).
 - [3] V.G.J. Stoks, R.A.M. Klomp, C.P.F. Terheggen, and J.J. de Swart, Phys. Rev. C **49**, 2950 (1994).
 - [4] W. Glöckle, H. Witała, D. Hüber, H. Kamada, and J. Golak, Phys. Rep. **274**, 107 (1996).
 - [5] H. Witała, W. Glöckle, J. Golak, A. Nogga, H. Kamada, R. Skibiński and J. Kuroś-Żolnierczuk, Phys. Rev. C **63**, 024007 (2001).
 - [6] J.L. Friar, B. F. Gibson, and G.L. Payne, Phys. Rev. C **37**, 2869 (1988).
 - [7] Y. Wu, S. Ishikawa, and T. Sasakawa, Few-Body Systems **15**, 145 (1993).
 - [8] A. Stadler, W. Glöckle, and P.U. Sauer, Phys. Rev. C **44**, 2319 (1991).
 - [9] A. Nogga, D. Hüber, H. Kamada, and W. Glöckle, Phys. Lett. **B409**, 19 (1997).
 - [10] M. R. Robilotta, Few-Body Systems, Suppl. **2**, 35 (1987).
 - [11] S. Weinberg, Phys. Lett. **B251**, 288 (1990).
 - [12] S. Weinberg, Nucl. Phys. **B363**, 3 (1991).
 - [13] U. van Kolck, Phys. Rev. C **49**, 2932 (1994).
 - [14] N. Kaiser, R. Brockmann, W. Weise, Nucl. Phys. **A625**, 758 (1997).
 - [15] E. Epelbaum, W. Glöckle, Ulf-G. Meissner, Nucl. Phys. **A671**, 295 (2000).
 - [16] E. Epelbaum, Ph.D. thesis, Ruhr-Universität, Bochum (2000).
 - [17] C. Ordóñez, L. Ray, and U. van Kolck, Phys. Rev. C **53**, 2086 (1996).
 - [18] P.F. Bedaque, H.-W. Hammer, U. van Kolck, Nucl. Phys. **A676**, 357 (2000).
 - [19] E. Epelbaum, Ulf-G. Meissner, W. Glöckle, C. Elster, H. Kamada, A. Nogga, H. Witała, in *Mesons and Light Nuclei*, edited by J. Adam, P. Bydzovsky, J. Mares (AIP Conf. Proc. No. 603, 2001), p. 17.
 - [20] D.R. Entem, R. Machleidt, nucl-th/0107057.
 - [21] E. Epelbaum, H. Kamada, A. Nogga, H. Witała, W. Glöckle, Ulf-G. Meissner, Phys. Rev. Lett. **86**, 4787 (2001).
 - [22] W. Polyzou, W. Glöckle, Few-Body Systems **9**, 97 (1990).
 - [23] S.A. Coon, M.D. Scadron, P.C. McNamee, B.R. Barrett, D.W.E. Blatt, and B.H.J. McKellar, Nucl. Phys. **A317**, 242 (1979).
 - [24] B.S. Pudliner, V.R. Pandharipande, J. Carlson, Steven C. Pieper, and R.B. Wiringa, Phys. Rev. C **56**, 1720 (1997).
 - [25] D. Hüber, H. Witała, H. Kamada, A. Nogga, W. Glöckle, Nucl. Phys. **A 631**, 663c (1998).
 - [26] H. Witała, W. Glöckle, J. Golak, D. Hüber, H. Kamada, A. Nogga, Phys. Lett. **B447**, 216 (1999).
 - [27] J.L. Friar, Few-Body Systems, Suppl. **1**, 94 (1986).
 - [28] R.B. Wiringa, Steven C. Pieper, J. Carlson, V.R. Pandharipande, Phys. Rev. C **62**, 014001 (2000).
 - [29] Steven C. Pieper, V.R. Pandharipande, R.B. Wiringa, J. Carlson, Phys. Rev. C **64**, 014001 (2001).
 - [30] P. Navrátil, G. P. Kamuntavičius, B.R. Barrett, Phys. Rev. C **61**, 044001 (2000).
 - [31] Y. Suzuki, K. Varga, *Stochastic variational approach to Quantum-Mechanical Few Body Problems*, vol. m54 of *Lecture Notes in Physics* (Springer-Verlag, Berlin, 1998).
 - [32] M. Viviani, A. Kievsky, and S. Rosati, Nuovo Cimento **631**, 111c (1992).
 - [33] H. Kameyama, M. Kamimura, and Y. Fukushima, Phys. Rev. C **40**, 974 (1989).
 - [34] N. Barnea, W. Leidemann, and G. Orlandini, Phys. Rev. C **61**, 054001 (2000).
 - [35] F. Ciesielski and J. Carbonell, Phys. Rev. C **58**, 58 (1998).
 - [36] H. Kamada and W. Glöckle, Nucl. Phys. **A548**, 205 (1992).
 - [37] A. Nogga, H. Kamada, W. Glöckle, Phys. Rev. Lett. **85**, 944 (2000).
 - [38] H. Kamada, A. Nogga, W. Glöckle, E. Hiyama, M. Kamimura, K. Varga, Y. Suzuki, M. Viviani, A. Kievsky, S. Rosati, R. B. Wiringa, Steven C. Pieper, J. Carlson, P. Navratil, B. R. Barrett, N. Barnea, W. Leidemann, G. Orlandini, Phys. Rev. C **64**, 044001 (2001).
 - [39] W. Glöckle and H. Kamada, Nucl. Phys. **A560**, 541 (1993).
 - [40] W. Glöckle and H. Kamada, Phys. Rev. Lett. **71**, 971 (1993).
 - [41] H. Kamada and W. Glöckle, Phys. Lett. **B 292**, 1 (1992).

- [42] H. Kamada and W. Glöckle, *Few Body Systems Suppl.* **7**, 217 (1994).
- [43] H. Kamada and W. Glöckle, in *AIP conference proceedings 334* (1994), p. 848.
- [44] TJLab, *Experiment e97-111*, (spokespeople J. Templon, J. Mitchell).
- [45] U. van Kolck, private communication.
- [46] S. Ramavataram, E. Hadjimichael, T.W. Donnelly, *Phys. Rev. C* **50**, 1175 (1994).
- [47] O. Yakubovsky, *Sov. J. Nucl. Phys.* **5**, 937 (1967).
- [48] A. Nogga, H. Kamada, W. Glöckle, in preparation.
- [49] W. Saake, master thesis, Ruhr-Universität Bochum (1992).
- [50] D. Hüber, H. Witała, A. Nogga, W. Glöckle, H. Kamada, *Few Body Systems* **22**, 107 (1997).
- [51] A. Nogga, Ph.D. thesis, Ruhr-Universität, Bochum (2001),
<http://www-brs.ub.ruhr-uni-bochum.de/netahtml/HSS/Diss/NoggaAndreas/>.
- [52] P.U. Sauer, *Prog. Part. Nucl. Phys.* **16**, 35 (1986).
- [53] J.L. Friar, G.L. Payne, V.G.J. Stoks, and J.J. de Swart, *Phys. Lett.* **B311**, 4 (1993).
- [54] A. Kievsky, M. Viviani, and S. Rosati, *Phys. Rev. C* **52**, R15 (1995).
- [55] A. Nogga, A. Kievsky, H. Kamada, W. Glöckle, L.E. Marcucci, S. Rosati, M. Viviani, *nucl-th/0202037*.
- [56] George Rupp and J.A. Tjon, *Phys. Rev. C* **45**, 2133 (1992).
- [57] F. Sammarruca, D.P. Xu, and R. Machleidt, *Phys. Rev. C* **46**, 1636 (1992).
- [58] A. Stadler, F. Gross, M. Frank, *Phys. Rev. C* **56**, 2396 (1997).
- [59] A. Stadler, F. Gross, *Phys. Rev. Lett.* **78**, 26 (1997).
- [60] W. Glöckle, T. S. H. Lee, F. Coester, *Phys. Rev. C* **33**, 709 (1986).
- [61] J. L. Forest, V. R. Pandharipande, A. Arriaga, *Phys. Rev. C* **60**, 014002 (1999).
- [62] L. L. Foldy and R. A. Krajcik, *Phys. Rev. Lett.* **32**, 1025 (1974).
- [63] S.A. Coon and M.T. Pena, *Phys. Rev. C* **48**, 2559 (1993).
- [64] S.A. Coon and H.K. Han, *Few Body Systems* **30**, 131 (2001).
- [65] A. Stadler, J. Adam Jr., H. Henning, and P.U. Sauer, *Phys. Rev. C* **51**, 2896 (1995).
- [66] B.H.J. McKellar and W. Glöckle, *Nucl. Phys.* **A416**, 435c (1984).
- [67] M. R. Robilotta, H. T. Coelho, *Nucl. Phys.* **A460**, 645 (1986).
- [68] J.L. Friar, D. Hüber, U. van Kolck, *Phys. Rev. C* **59**, 53 (1999).
- [69] A. Kievsky, private communication.
- [70] J.L. Friar, B. F. Gibson, and G.L. Payne, *Phys. Rev. C* **35**, 1502 (1987).
- [71] J.A. Tjon, *Phys. Lett. B* **56**, 217 (1975).
- [72] J.L. Friar, B. F. Gibson, G.L. Payne, and S. A. Coon, *Few Body Systems* **5**, 13 (1988).
- [73] T. Sasakawa and S. Ishikawa, *Few Body Systems* **1**, 3 (1986).
- [74] A. Bömelburg, *Phys. Rev. C* **34**, 14 (1986).
- [75] J. L. Forest, V. R. Pandharipande, Steven C. Pieper, R. B. Wiringa, R. Schiavilla, A. Arriaga, *Phys. Rev. C* **54**, 646 (1996).
- [76] W. Glöckle, H. Kamada, J. Golak, A. Nogga, H. Witała, R. Skibiński, J. Kuroś-Żolnierczuk, *Acta Physica Polonica* **B32**, 3053 (2001).
- [77] J. Ryckebusch *et. al.*, *Nucl. Phys.* **A624**, 581 (1997).
- [78] G. Rosner, *Progr. in Part. and Nucl. Phys.* **44**, 99 (2000).
- [79] J.J. van Leeuwe *et. al.*, *Phys. Rev. Lett.* **80**, 2543 (1998).
- [80] S. A. Sofianos, G. Ellerkmann, W. Sandhas, *nucl-th/9909063*.
- [81] O. Benhar, N.N. Nikolaev, J. Speth, A.A. Usmani, B.G. Zakharov, *Nucl. Phys.* **A673**, 241 (2000).
- [82] H. Morita and T. Suzuki, *Prog. of Theor. Phys.* **86**, 671 (1991).
- [83] L.L. Frankfurt, M.M. Sargsian, M.I. Strikman, *Phys. Rev. C* **56**, 1124 (1997).
- [84] E. Epelbaum, A. Nogga, W. Glöckle, H. Kamada, Ulf.-G. Meißner, H. Witała, *nucl-th/0201064*.